Opto-Electronics Review 28 (2020) 69–73

PAN POLISH ACADEMY OF SCIENCES

Opto-Electronics Review

journal homepage: http://journals.pan.pl/opelre

Investigation of rotational motion in a reinforced concrete frame construction by a fiber optic gyroscope

A. T. Kurzych[a*], L. R. Jaroszewicz[a], J. K. Kowalski[b], B. Sakowicz[c]

[a]Institute of Technical Physics, Military University of Technology, 2 gen. S. Kaliskiego St., Warsaw 00-908, Poland
[b]Elproma Elektronika Ltd., 13 Szymanowskiego St., Łomianki 05-092, Poland
[c]Dep. of Microelectronics and Computer Science, Lodz University of Technology, 221/223 Wólczańska St., Lodz 90-924, Poland

Article info

Article history:
Received 25 Mar. 2020
Received in revised form 01 Apr. 2020
Accepted 01 Apr. 2020

Keywords:
rotational seismology, fiber-optic rotational seismometer, civil engineering, sensors

Abstract

This paper deals with an issue of a rotational motion impact on a construction and presents civil engineering applications of a fiber optic rotational seismograph named Fiber-Optic System for Rotational Events & Phenomena Monitoring. It has been designed for a long- term building monitoring and structural rotations' recording. It is based on the Sagnac effect which enables to detect one-axis rotational motion in a direct way and without any reference system. It enables to detect a rotation component in the wide range of a signal amplitude from 10^{-8} rad/s to 10 rad/s, as well as a frequency from DC to 1000 Hz. Data presented in this paper show the behavior of a reinforced concrete frame construction on different floors. Several measurements were carried out by placing the applied sensor on different floor levels of a building. The laboratory and in-situ measurements confirmed that Fiber-Optic System for Rotational Events & Phenomena Monitoring is an accurate and suitable device for applications in civil engineering.

1. Introduction

Building structures are constantly exposed to all sorts of dynamic impacts, source of which can be both natural phenomena occurring on the Earth's surface (e.g., wind load) and below its surface caused by movements of the Earth's crust, as well as vibrations caused by human activity. An important aspect of designing building structures is a correct assessment of a vibration impact on the building, as well as selection of an appropriate security technology to minimize undesirable effects caused by dynamic interactions.

Until recently, there have been only three components of a linear soil movement measured in the seismology and seismic engineering (along two horizontal *x*, *y* and *z*-axes). Only these three degrees of freedom, which are associated with the translational motion or acceleration along the Cartesian reference frame, have been recorded by different sensors such as seismometers or accelerometers [1]. Such approach indirectly neglects rotation motion components. The three rotation components have been neglected because of lack of appropriate and accurate devices. However, it turned out that three additional rotational degrees of freedom during measurements of ground vibrations can provide new information valuable for seismological society [2-5]. They can help to understand Earth's inner structure, seismic sources, as well as they are significant for engineering [6,7], e.g., high-rise buildings' or wind farms' monitoring. Moreover, research of a character regarding near-filed ground movements is significant for earthquake engineers interested in a seismically safe designing, as well as for seismologists investigating physical processes leading to the ground-motion complexity [8].

Generally, one can extinguish six motions: three translations of $u_x(t)$, $u_y(t)$ and $u_z(t)$ along *x*-, *y*-, and *z*-axes and three rotations of Ω_x, Ω_y and Ω_z around these axes [9] (see Fig. 1). The rotation around the vertical axis (Ω_z) is usually called a torsion, while the rotations around the horizontal axes (Ω_x, Ω_y) are called rocking [10]. Torsion may be the result of an S-wave propagation, as well as a Love wave, while rocking is the result of a P- and Rayleigh wave propagation [10].

*Corresponding author at: anna.kurzych@wat.edu.pl

https://doi.org/10.24425/opelre.2020.132503

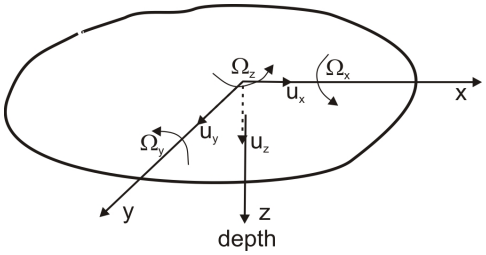

Fig. 1. Sketch showing directions of a translational and rotational motion on the ground surface [9].

The aim of this work is to characterize the performance of an interferometric fiber optic rotational seismograph - Fiber-Optic System for Rotational Events & Phenomena Monitoring (FOSREM) - which has been designed to register rotational phenomena in engineering constructions. It is based on a well-known Sagnac effect and allows to record angular velocity in the wide range of an amplitude (10^{-8} rad/s – 10 rad/s), as well as a frequency content (DC to 1000 Hz). Since the system has also a compact hermetically sealed construction, FOSREM fulfills all requirements of rotational seismology due to the above parameters [9].

2. FOSREM construction

FOSREM is a highly developed optical interferometer for a high-resolution readout of the Sagnac phase shift [11] induced between two counterpropagating waves in the closed optical path when the plane of propagation undergoes angular velocity [12,13]. The general construction of FOSREM can be divided in two parts which operate dependently: optical and electronic. The optical part is based on the minimum gyro configuration with a 5 000 m SMF-28e+ (*Corning Inc.*, USA) sensor loop and MIOC - Multi-Integrated Optical Circuit unit (*IdealPhotonics Ltd.*, China). It used also other telecommunication fiber-optic components such as: isolator, depolarizer, X-type coupler and polarizer coupled together via fused splices in the structure shown in Fig. 2 with total optical losses equal to 19.63 dB. A superluminescent diode is applied as a light source with the optical power P = 10 mW, the central wavelength λ = 1311.2 nm and the beamwidth of 51.2 nm (*Exalos AG*, Switzerland), whereas as a detector the InGaAs avalanche photodiode APD1310 (*Optoway*, Taiwan) has been applied. In opposite to our previous work [9] FOSREM operates in a closed-loop configuration [14] which is produced by a new electronic part (see Fig. 2). The electronic part consists of the following modules: SLED driver (*Exalos AG*, Switzerland), four-step modulator for MIOC driving, analogue amplifier for APD, control modules based on FPGA (processing data from sensor and performing necessary calculations and filtration), power module (uses 24VAD/20W via PCU – Power and Communication Unit). This internal digital processing unit provides a rotation speed value directly in a digital form. FOSREM has an RS-485 interface for data and USB interface for diagnostic [see Fig. 3(b)]. The connection provides data transmission and power supply from PCU over only one standard M12 cable within the distance of 500 m. PCU is connected to the Internet over the Ethernet or WiFi local networks, or 3G/4G mobile networks. The

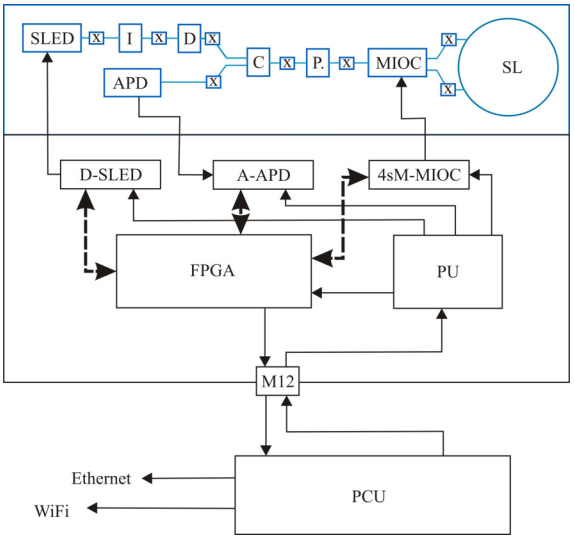

Fig. 2. Scheme of FOSREM: top – optical part, bottom – electronic part. Symbols: SLED – light source, I – fiber-optic isolator, D – fiber-optic depolarizer, C – fiber-optic coupler X-type, P – fiber-optic polarizer, MIOC – multi-integred optical circuit, SL – sensor loop, X – fused splice, APD – avalanche photodetector, D-SLED – SLED driver, A–APD – APD amplifier, 4sM-MIOC – four-step MIOC modulator, FPGA – general FPGA unit, PU – power unit, PCU – power and communication unit.

system provides the VPN functionality, thanks to this, one can connect multiple sensors in one large, synchronized network and, thus monitor a big number of sensors from a single location. FOSREM operates with a 1 ms sampling rate which secures 1000 sps data transfer as in Ref. 15.

The whole idea of a FOSREM construction was to design a portable, remote and resistant to external conditions sensor. For that reason, the authors designed a compact and integrated device with a diameter equal to 312 mm and a height equal to 85 mm as is shown in Fig. 3. Moreover, in order to apply the sensor in all environmental conditions, it is hermetically sealed and equipped with waterproof connectors meeting the IP67 requirements [see Fig. 3(b)].

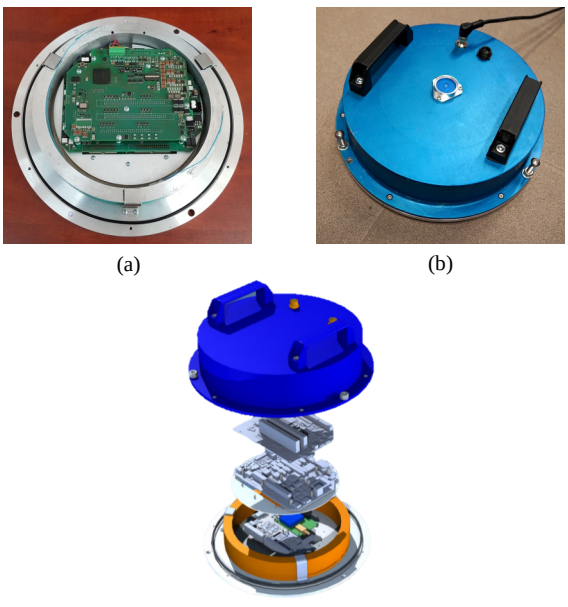

(a) (b)

(c)

Fig. 3. FOSREM construction: (a) view of the sensor's inner, (b) view of the sensor's outer, (c) sensor's 3D project.

In order to verify the sensor's parameters and resistance to temperature changes, there was the Allan variance analysis [16] carried out along with measurements in a climatic chamber 7010 (*Vötsch*, Germany). During the FOSREM's temperature resistant research, the range of temperature was from -10°C to 50°C and every 10°C the sensor was heated for an hour in order to stabilize the conditions. The collected signal is continuous [Fig. 4(a)] where observed disturbances [Fig. 4(b)] were caused mainly by the climatic chamber which generates vibrations, as well as airflow. Nevertheless, the relative error even with disturbances generated by a climatic chamber operation does not exceed 4.5%, so it can be concluded as a proper result [Fig. 4(c)].

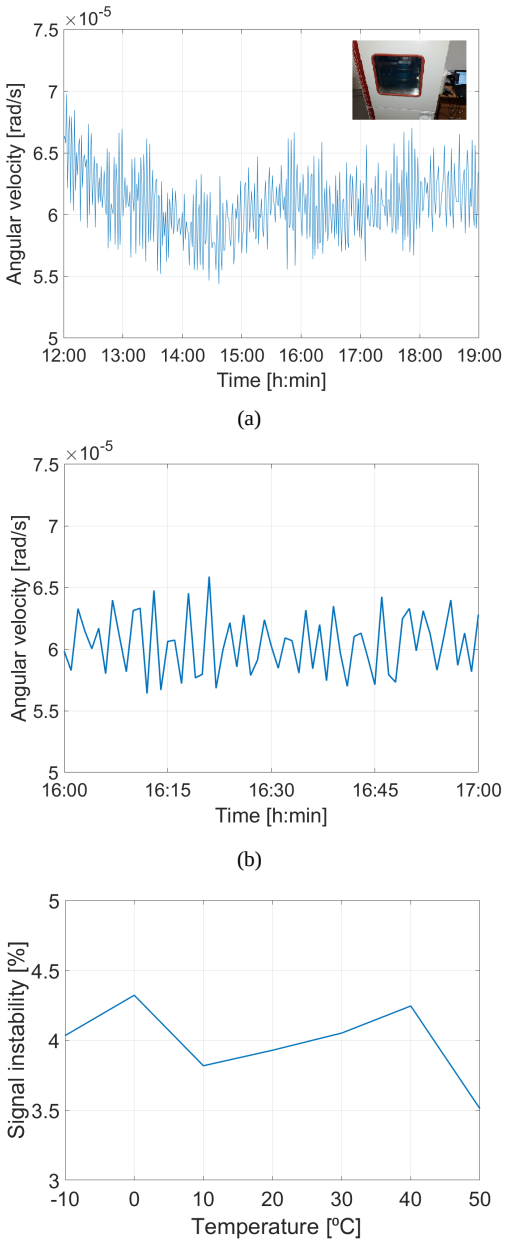

Fig. 4. Measurements in the climatic chamber: (a) signal collected by FOSREM during the climatic chamber operating in the range of -10°C to 50°C with the general chamber view in top inside picture, (b) signal collected for temeperature changes between 30°C – 40°C (c). The calculated singal instability is based on the relative error in particular temperature.

During data gathering for the Allan variance analysis it is required to install a tested sensor in isolated conditions, otherwise determined parameters will be incorrect. Initially for the Allan variance analysis FOSREM has been installed in the laboratory environment, in the basement. FOSREM has been positioned to measure only torsions and data were recorded during night hours in order to avoid urban noises. The determined Allan variance curve is presented in Fig. 5(a). On this basis primary parameters were determined: angle random walk equalling $1.23 \cdot 10^{-6}$ rad/√s and bias instability equalling $5.35 \cdot 10^{-8}$ rad/s. As one can see same noise sources with frequencies in the range of a few hertz existing in such conditions, manifested as observed nonlinearity of a curve in Fig. 5(a) for a sample period of about 1 s, have influence on the obtained results. In order to reduce disturbances during data gathering, the authors installed FOSREM on an active optical table PFA5250 (*Thorlabs*, Sweden). The Allan variance curve based on the data when FOSREM has been placed in the active optical table is presented in Fig. 5(b). One can see that the curve has more theoretical course and the parameters determined basing on this data are as follows: angle random walk equals $3.24 \cdot 10^{-7}$ rad/√s and bias instability equals $2.55 \cdot 10^{-8}$ rad/s. It should be noticed that for the horizontal positioning system the torsion connected with Earth's rotation for Warsaw latitude is of $\Omega_z = 4.45 \cdot 10^{-5}$ rad/s and it can be treated as constant because the dimensionless variation of the angular rotation rate ($d\Omega_z/\Omega_z$) is equal to 10^{-8} [17].

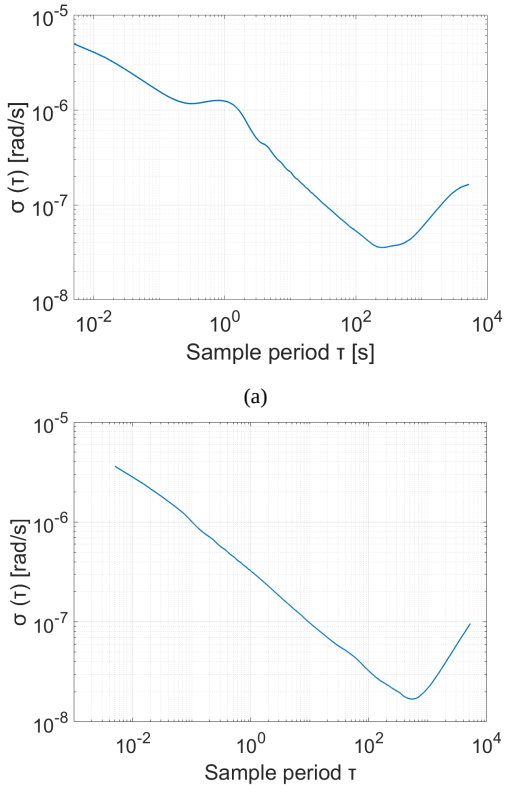

Fig. 5. FOSREM's Allan variance analysis: (a) curve determined basing on data gathered when FOSREM was istalled in the laboratory enviroment, (b) curve determined basing on data gathered when FOSREM was installed in the active optical table.

The curves presented in Fig. 5 underline that environmental conditions during data gathering for the Allan variance analysis are crucial and can lead to an incorrect result. For the above reason the obtained results basing on Fig. 5(b) should be taken into consideration and they are satisfactory.

3. Results

The building under investigation is located at the area of Military University of Technology, Warsaw, Poland and has number 100 [Fig. 6(a)]. It was built in the 1960s. Its construction is a reinforced concrete skeleton with reinforced concrete girders and floor slabs based on girders. The outer walls fill the reinforced concrete skeleton structure using silicate bricks with plaster on both sides. There is a single carriageway with a lane for trams in the distance of about 123 m from the building. Sensors were located at the building's corner from where the distance to the road is of about 160 m as is shown in Fig. 6(b). During experiment FOSREMs were positioned horizontally by using a suitable screw and a bullseye spirit bubble level [see Fig. 3(b)] for measuring only a torsion.

(a)

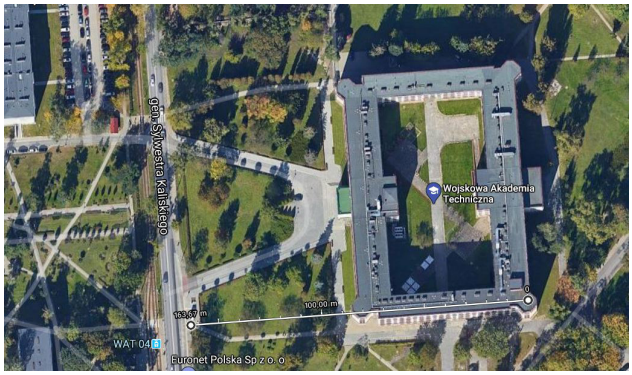

(b)

Fig. 6. The analysed building number 100 of Military University of Technology, Warsaw, Poland: (a) view from the entrance, (b) satellite image indicating the distance from the sensor to the street.

Data were collected in long-term night hours in order to reduce impact of urban noises and disturbances induced by workers and they are presented in Fig. 7 and Table 1. It should be underlined that presented data contain the constant rotation rate connected with Earth's rotation ($\Omega_z = 4.45 \cdot 10^{-5}$ rad/s) which cumulates the measured angular value on each floor.

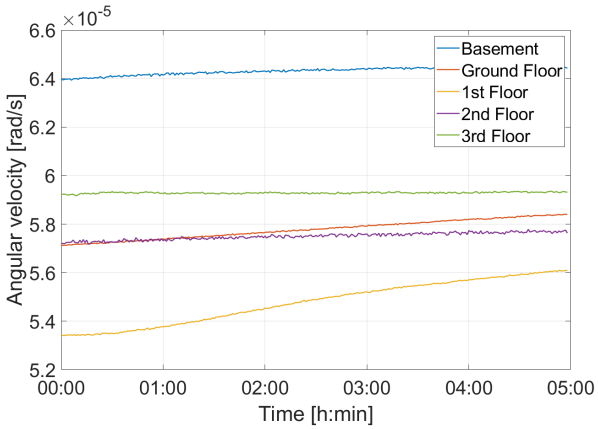

Fig. 7. Data gathered by FOSREM on a particular floor of the analysed building number 100 of Military University of Technology, Warsaw, Poland.

The presented data in Fig. 7 points out that the maximum value of angular velocity has been recorded by FOSREM in the basement and it equals $6.430 \cdot 10^{-5} \pm 0.002 \cdot 10^{-5}$ rad/s (Table 1). Table 1 presents the average value of angular velocity for each floor. Data were collected with a 1 ms sampling rate, however, in order to avoid big size of files, FOSREM's system has function which gives an averaged value of angular velocity every minute. The presented standard deviation is given for this averaging time and these values approximately correspond with a standard deviation for data collected during each hour, except data on ground and the first floor where growing rotation speed is observed in the morning. Changes in the signal exactly on these floors are caused by building actions while other floors accumulated the energy of vibration.

Table 1
The recorded amplitude of the signal on the particular floor.

Floor	Average value of angular velocity [rad/s]	Standard deviation [rad/s]
Basement (-0.75 m high)	$6.430 \cdot 10^{-5}$	$0.002 \cdot 10^{-5}$
Ground Floor* (0.00 m high)	$5.725 \cdot 10^{-5}$ $5.830 \cdot 10^{-5}$	$0.006 \cdot 10^{-5}$ $0.007 \cdot 10^{-5}$
1st Floor* (+3.20 m high)	$5.354 \cdot 10^{-5}$ $5.590 \cdot 10^{-5}$	$0.011 \cdot 10^{-5}$ $0.008 \cdot 10^{-5}$
2nd Floor (+7.00 m high)	$5.750 \cdot 10^{-5}$	$0.005 \cdot 10^{-5}$
3rd Floor (+10.80 m high)	$5.929 \cdot 10^{-5}$	$0.001 \cdot 10^{-5}$

*Since the rotation rate is growing with time for these floors, average value of angular velocity is calculated for the first and last hour of the measurement.

The amplitude decreases as the height of the building increases. The theoretical assumptions that the building structure eliminates vibrations on the upper floors is confirmed, but only up to the 3rd floor where the amplitude starts to grow. Probably, it is caused by the fact that it is top level and nothing from the building structure stabilizes its works on this level. The growing amplitude of angular velocity for this level for morning hours correlated with the

ground floor data can be connected to increased sources of vibration caused by urban activity.

In the analyzed example of the building it is difficult to define a source of vibrations which can be among others: operation of machines and mechanical devices located in the building and outside it, passing of wheeled trams vehicles (traffic vibrations, it is very possible because of the distance from the place of data gathering and the road which equals about 160 m), construction works (including driving diaphragm walls and foundation piles into the ground), as well as environmental conditions, e.g., strong wind. Passage of vehicles weighing from a dozen to several dozen tons contributes to the formation of vibrations propagating in all directions. The formed waves in the ground get into the foundation transferring to the entire structure. It can explain the maximum value of angular velocity in the basement. It should be mentioned that dynamic actions are additional load on buildings that should be included in their strength calculations. The assessment of the vibrations' impact is based on the consideration of their harmfulness on structures and people inside the building.

4. Conclusions

Nowadays, building structures are constantly exposed to various kinds of dynamic impact, resulting from both continuous technological developments, the need to erect higher and higher buildings, but also from natural phenomena occurring on the surface of the Earth.

The paper presents the application of the fiber optic rotational seismograph used for a rotational motion monitoring in the constructions. The recorded angular velocity on a different floor of the reinforced concrete frame building construction indicates that the building attenuates vibration with increasing height up to the 3rd floor. The signal maximum amplitude has been recorded in the basement.

The carried experiment, as well as the laboratory investigation confirmed that FOSREM is a suitable device for continuous monitoring of engineering structures. It is mobile, as well as remotely controlled by the Internet. Its range of measurement (amplitude of 10^{-8} rad/s - 10 rad/s; frequency of DC to 1000 Hz) allows to apply it in a wide range of rotational seismology area of interest, such as investigation of natural sources of rotational events (earthquakes, volcano activity, etc.) and engineering structures.

Author's statement

A. T. Kurzych, L. R. Jaroszewicz: FOSREM's optical part construction and article preparation, as well as research conducting; J. K. Kowalski, B. Sakowicz: FOSREM's electronic part construction and data processing.

Acknowledgements

This work was financially supported by the National Science Centre, Poland – project no. 2016/23/N/ST10/02508, as well as program POIR 04.02.00-14-A003/16 "EPOS - System Obserwacji Płyty Europejskiej".

References

[1] Havskov, J., Alguacil, G. *Instrumentation in Earthquake Seismology*, 2nd ed. (Springer: Cham, Switzerland, 2016).

[2] Huang, B. S. Ground Rotational Motions of the 1991 Chi-Chi, Taiwan, Earthquake Asinferred from Dense Array Observations. *Geophys. Res. Lett*. **30** (6), 1307–1310 (2003). https://doi.org/10.1029/2002GL015157.

[3] Igel, H., Schreiber, U., Flaws, A., Schuberth, B., Velikoseltsev, A., Cochard, A. Rotational Motions Induced by the M8.1 Tokachi-Oki Earthquake, September 25, 2003, *Geophys. Res. Lett*. **32**, (2005). https://doi.org/10.1029/2004GL022336.

[4] Igel, H., Cochard, A., Wassermann, J., Flaws, A., Schreiber, U., Velikoseltsev, A., Pham Dinh, N. Broad-Band Observations of Earthquake-Induced Rotational Ground Motions, *Geophys. J. Int.* **168** (1), 182–196 (2007). https://doi.org/10.1111/j.1365-246X.2006.03146.x.

[5] Takeo, M. Ground Rotational Motions Recorded in Near- Source Region of Earthquakes, in *Earthquake Source Asymmetry, Structural Media and Rotation Effects* (eds. Teisseyre, R., Takeo, M., Majewski, E.) 157–167 (Springer-Verlag Berlin Heidelberg, 2006).

[6] Trifunac, M. D. A Note on Rotational Components of Earthquake Motions on Ground Surface for Incident Body Waves, *Int. J. Soil Dyn. Earthq. Eng.* **1** (1), 11–19 (1982). https://doi.org/10.1016/0261-7277(82)90009-2.

[7] Trifunac, M. D. Effects of Torsional and Rocking Excitations on the Response of Structures. in *Earthquake Source Asymmetry, Structural Media and Rotation Effects* (eds. Teisseyre, R., Takeo, M., Majewski, E.) 569–582(Springer-Verlag Berlin Heidelberg, 2006).

[8] Mai, P. Ground Motion: Complexity and Scaling in the Near Field of Earthquake Ruptures. in *the Near Field of Earthquake Ruptures* (eds. Meyers R.) 623–662 (Springer, New York, 2011).

[9] Jaroszewicz, L. R., Kurzych, A. T., Krajewski, Z., Marć, P., Kowalski, J. K., Bobra, P., Zembaty, Z., Sakowicz, B., Jankowski R. Review of the Usefulness of Various Rotational Seismometers with Laboratory Results of Fibre-Optic Ones Tested for Engineering Applications, *Sensors* **16** (12), 2161 (2016), https://doi.org/10.3390/s16122161

[10] Zembaty, Z. Numerical Analyses of Seismic Ground Rotations from the Wave Passage Effects. in *Seismic Behaviour and Design of Irregular and Complex Civil Structures* (eds. Lavan, O., De Stefano, M.) 15–28 (Springer, 2013).

[11] Sagnac, G. L'éther Lumineux Démontré Par l'effet Du Vent Relatif d'éther Dans Un Interféromètre En Rotation Uniforme, *Compte-Rendus À L'Académie Sci.* **95**, 708-10 (1913).

[12] Post, E. J. Sagnac Effect, *Rev Mod Phys* **39** (2), 475–493 (1967). https://doi.org/10.1103/RevModPhys.39.475.

[13] Michelson, A. A., Gale, H. G. The Effect of the Earth's Rotation on the Velocity of Light, *Nature* **115**, 566–566 (1925). https://doi.org/10.1038/115566a0.

[14] Lefèvre, H. C. *The Fiber-Optic Gyroscope*, 2nd ed., Chap. 8 (Artrech House, United Kingdom, 2014).

[15] Jaroszewicz, L. R. Kurzych, A. T. Krajewski, Z. Teisseyre, K. Dudek, M. Kowalski, J. K. Experimental Perspectives for Rotational Seismology – Construction of Optical Fiber Sensors Set, *5th worksop of International Working Group on Rotational Seismology, IWGoRS Workshop* (2019).

[16] Freescale Semiconductor, Inc., Allan Variance: Noise Analysis for Gyroscopes (2005).

[17] Levin, B. W., Sasorova, E. V., Steblov, G. M., Domanski A. V., Prytkov, A. S., Tsyba, E. N. Variations of the Earth's Rotation Rate and Cyclic Processes in Geodynamics, *Geodesy and Geodynamics* **8,** 206–212 (2017). https://doi.org/10.1016/j.geog.2017.03.007.